**Electrocatalytic Water Oxidation** 

www.afm-journal.de

# Oxygen Evolution Reaction on 2D Ferromagnetic Fe<sub>3</sub>GeTe<sub>2</sub>: Boosting the Reactivity by the Self-Reduction of Surface Hydroxyl

Yinghe Zhao, Jinxing Gu, and Zhongfang Chen\*

This paper is dedicated to Professor Walter Thiel on the occasion of his 70th birthday

Fe<sub>3</sub>GeTe<sub>2</sub> is a water- and air-stable, metallic, and layered material. Very recently, few-layer and single-layer Fe<sub>3</sub>GeTe<sub>2</sub> have been successfully exfoliated from its bulk and revealed as 2D ferromagnets (*Nature* 2018, *563*, 94; *Nat. Mater.* 2018, *17*, 778). Here, the basal plane of Fe<sub>3</sub>GeTe<sub>2</sub> is demonstrated to be of high electrocatalytic activity towards oxygen evolution reaction (OER) without resorting to any chemical modifications, by means of systematic density functional theory computations. The Fe<sub>3</sub>GeTe<sub>2</sub> nanosheet preserves the metallic character of the bulk, and its 2D layered structure provides abundant exposed active sites to catalyze OER. All these unique characteristics suggest that the Fe<sub>3</sub>GeTe<sub>2</sub> nanosheet may be an excellent catalyst for electrochemical OER. More importantly, it is found that the self-reduction of surface hydroxyl into water can significantly reduce the overpotential for OER, which greatly boosts the OER activity. This work not only reveals new mechanisms for OER but also opens the door for the application of emerging 2D ferromagnets in the field of energy storage and conversion.

#### 1. Introduction

Electrochemical water oxidation, also denoted as oxygen evolution reaction (OER), is a critical reaction in many energy storage and conversion technologies, such as water splitting and metal-air batteries.<sup>[1-10]</sup> OER is intrinsically a four-electron and uphill reaction, leading to a large overpotential and sluggish kinetics. An electrocatalyst is required to decrease the overpotential and speed OER up.<sup>[1-10]</sup> The design of electrocatalysts mainly follows two parallel frontiers—homogeneous and heterogeneous catalysis, each of which has its own advantages and drawbacks.<sup>[11,12]</sup> High atom utilization efficiency renders homogeneous electrocatalysts intriguing, but poor durability and recyclability impede their applications. In contrast, heterogeneous electrocatalysts are of excellent stability and recyclability, and easy to be integrated with electrodes. However, the limited surface area of heterogeneous electrocatalysts to

Dr. Y. Zhao, J. Gu, Prof. Z. Chen Department of Chemistry University of Puerto Rico San Juan, PR 00931, USA E-mail: zhongfangchen@gmail.com

The ORCID identification number(s) for the author(s) of this article can be found under https://doi.org/10.1002/adfm.201904782.

DOI: 10.1002/adfm.201904782

contact with reaction intermediates usually results in a rather low atom utilization efficiency.

Since the discovery of graphene,<sup>[13]</sup> 2D van der Waals (vdW) materials have emerged as new frontiers of electrocatalysts.[14-18] With extremely high specific surface areas, the electrocatalysts based on 2D vdW materials combine the advantages of both homogeneous and heterogeneous catalysts. Unfortunately, the large-area basal planes of most pristine 2D vdW materials are inert towards electrochemical reactions, and surface modifications, such as doping,[19-34] interfacial engineering,[35-37] and defect engineering,[14,38-44] are often required to use the basal planes as catalytic active sites. Remarkably, if the basal plane of a metallic 2D vdW material has high OER activity without resorting to any surface

modifications, it will significantly promote the development of the OER-related energy technologies.

The newly discovered vdW materials may offer excellent candidates for us to achieve high-performance metallic 2D electrocatalysts for OER. Especially, ferromagnetic ordering has been experimentally observed in bilayer Cr<sub>2</sub>Ge<sub>2</sub>Te<sub>6</sub><sup>[45]</sup> and monolayer CrI<sub>3</sub><sup>[46]</sup> exfoliated from their bulks, making 2D vdW ferromagnets a new horizon in materials science. [47-50] These new materials not only could be excellent candidates, but also may refresh our understanding to the reaction mechanisms. Interestingly, the electrochemical performance of magnetic materials can be further enhanced under an external magnetic field.<sup>[51-54]</sup> Therefore, it is highly desirable to explore whether the emerging 2D vdW ferromagnets can be used as OER electrocatalysts. In contrast to Cr<sub>2</sub>Ge<sub>2</sub>Te<sub>6</sub>,<sup>[45]</sup> CrI<sub>3</sub>,<sup>[46]</sup> and some newly proposed 2D vdW ferromagnets, [55–57] Fe<sub>3</sub>GeTe<sub>2</sub> shows metallic character due to itinerant electrons.<sup>[58-60]</sup> Providing that the basal plane of Fe<sub>3</sub>GeTe<sub>2</sub> owns high OER activity, Fe<sub>3</sub>GeTe<sub>2</sub> will have great potential to be an excellent electrocatalyst towards OER.

In this work, by means of density functional theory (DFT) calculations, we systematically explored the potential of Fe<sub>3</sub>GeTe<sub>2</sub> nanosheet as an OER electrocatalyst. Our computations revealed that the basal plane of Fe<sub>3</sub>GeTe<sub>2</sub> exhibits high activity towards OER with an overpotential of 0.30 V, the OER activity and metallicity of Fe<sub>3</sub>GeTe<sub>2</sub> are independent of the spin orientation, and the metallic behavior of Fe<sub>3</sub>GeTe<sub>2</sub> can be well

www.afm-journal.de

preserved from bulk to single layer. The high OER activity and metallicity, together with the 2D layered structure, endow Fe<sub>3</sub>GeTe<sub>2</sub> nanosheet great potential as a high-performance OER electrocatalyst. Remarkably, we found that the self-reduction of surface hydroxyl into water plays a crucial role in lowering the OER overpotential. Such new insights not only underscore the importance of surface hydroxyl in OER and gain us new understanding towards the reaction mechanisms, but also may guide further development of efficient OER electrocatalysts.

#### 2. Results and Discussion

# 2.1. Geometric Structure and Electronic and Magnetic Properties of Fe<sub>3</sub>GeTe<sub>2</sub>

Fe<sub>3</sub>GeTe<sub>2</sub>, first synthesized by Deiseroth and co-workers in  $2005,^{[61,62]}$  is a water and air-stable layered material with good thermal stability (thermal decomposition occurs at over 800 °C). [62] Magnetic measurements revealed that that Fe<sub>3</sub>GeTe<sub>2</sub> is ferromagnetic with high Curie temperature and itinerant magnetism.<sup>[61-63]</sup> According to our computations, the magnetic moment of Fe<sub>3</sub>GeTe<sub>2</sub> is dominantly contributed by the Fe atoms, and its magnetic moment is 1.49  $\mu_B$  per Fe atom, in good agreement with previous experimental and theoretical studies. [61,63,64] Fe<sub>3</sub>GeTe<sub>2</sub> consisting of an ABAB stacking has a hexagonal symmetry with a space group of P63/mmc (no. 194) (see Figure S1, Supporting Information). The optimized lattice parameters are a = b = 3.89 Å, and c = 15.87 Å, which agree well with the previous explorations.<sup>[64]</sup> The distance between A and B layers, namely the nearest interlayer distance h (Figure S1, Supporting Information), is around 3.0 Å, while the nearest Te-Te distance between two adjacent layers is slightly over 3.5 Å, both of which are in the typical vdW interaction range.

Excitingly, the exfoliation of few- and single-layer Fe<sub>3</sub>GeTe<sub>2</sub> has been achieved by Zhang's[58] and Xu's groups.[59] The Fe<sub>3</sub>GeTe<sub>2</sub> monolayer consists of two Te sublayers, two Fe sublayers, and one mixed sublayer of Fe and Ge atoms (Figure 1a). Figure S2 of the Supporting Information shows charge density distributions of the optimized Fe<sub>3</sub>GeTe<sub>2</sub> monolayer in the spin-up and spin-down channels. Note that the Fe atoms in the monolayer are located in two inequivalent Wyckoff sites, denoted as Fe<sub>I</sub> in the Fe sublayer and Fe<sub>II</sub> in the mixed sublayer. Our DFT computations showed that the magnetic moment of  $Fe_I$  is ca. 0.7  $\mu_B$  larger than that of  $Fe_{II}$ , which agrees with the previous study. [64] The valence states of Fe<sub>3</sub>GeTe<sub>2</sub> can be regarded as  $(Te^{2-})(Fe_1^{3+})[(Fe_1^{2+})(Ge^{4-})](Fe_1^{3+})(Te^{2-})$ . The contribution of all atomic orbitals is shown in Figure S3 of the Supporting Information. Each Te atom is bound to four Fe atoms, including three Fe<sub>I</sub> atoms and one Fe<sub>II</sub> atom. One Te atom and three Fe<sub>I</sub> atoms constitute a trigonal pyramidal. The Te-Fe<sub>II</sub> bond is just perpendicular to the mixed sublayer consisting of  $Fe_{II}$  and Ge atoms. Ge and  $Fe_{II}$  atoms form a graphene-like honeycomb structure in the mixed sublayer. Each Ge atom is also connected to six Fe<sub>1</sub> atoms. From bulk to single layer, the hexagonal symmetry is maintained in Fe<sub>3</sub>GeTe<sub>2</sub>. The optimized lattice parameters of single-layer  $Fe_3GeTe_2$  is a = b = 3.91 Å, in line with the previous exploration.<sup>[64]</sup> The bond length can be found in Table S1 of the Supporting Information, and the bond

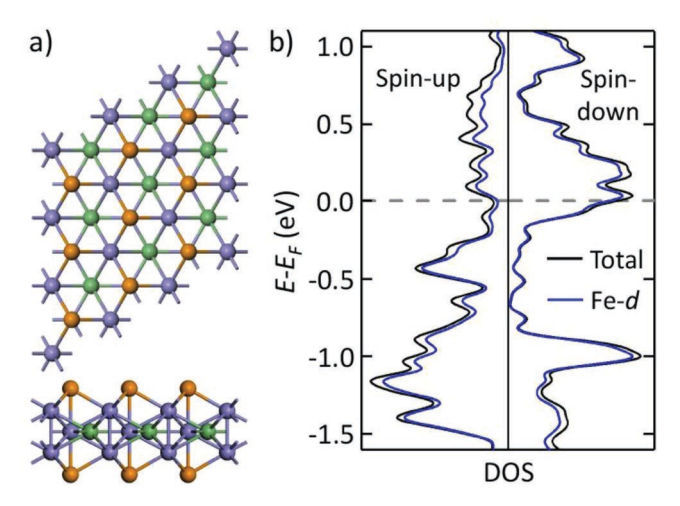


**Figure 1.** a) Top and side views of the  $Fe_3GeTe_2$  monolayer where Te, Fe, and Ge atoms are denoted by red, blue, and green balls, respectively. b) Spin-polarized PDOS of single-layer  $Fe_3GeTe_2$  with respect to Fermi level ( $E_F$ ). The DOS ranges in the spin-up and spin-down channels are 0.0–7.0 and –9.0 to 0.0, respectively.

angle can be derived by visualizing the structure (Table S2, Supporting Information).

Metallicity that allows the high-speed transport of electrons is an important precondition of high-performance electrocatalysts.[14,15] The computed density of states (DOS) of bulk Fe<sub>3</sub>GeTe<sub>2</sub> (Figure S4a, Supporting Information) confirms its metallic character as revealed experimentally.[61,63] Bulk Fe<sub>3</sub>GeTe<sub>2</sub> exhibits metallic behavior both in the spin-up and spin-down channels, and the projected DOS (PDOS) analysis demonstrates that the metallicity is mainly contributed by Fe's d orbitals. Though the bulk Fe<sub>3</sub>GeTe<sub>2</sub> is metallic, this does not ensure the metallic character of few- or single-layer Fe<sub>3</sub>GeTe<sub>2</sub>, since the electronic properties of 2D vdW materials are often dependent on the layer number.<sup>[65-73]</sup> For example, the bandgap of black phosphorus nanosheets decreases with increasing the thickness. [65-67] For some layered materials, even a metal-semiconductor transition can occur with reducing the layer number.<sup>[68,71,72]</sup> Thus, we examined the electronic properties of Fe<sub>3</sub>GeTe<sub>2</sub> nanosheets with different thickness. Fortunately, Fe<sub>3</sub>GeTe<sub>2</sub> remains metallic upon exfoliation: trilayer, bilayer, and single-layer Fe<sub>3</sub>GeTe<sub>2</sub> are all metallic according to the DOS analysis (Figure S4b,c, Supporting Information and Figure 1b), and their DOS show similar profiles with the bulk DOS around the Fermi level (Figure S4a, Supporting Information).

#### 2.2. OER Activity of Fe<sub>3</sub>GeTe<sub>2</sub> along the Classical Pathway

Next, we will explore whether the basal plane of Fe<sub>3</sub>GeTe<sub>2</sub> owns high OER activity. First, we examined OER following the classical pathway:  $^{[74]}$ \* + OH $^ \rightarrow$  OH\* + e $^-$  (1), OH\* + OH $^ \rightarrow$  O\* + H<sub>2</sub>O + e $^-$  (2), O\* + OH $^ \rightarrow$  OOH\* + e $^-$  (3), OOH\* + OH $^ \rightarrow$  OO\* + H<sub>2</sub>O + e $^-$  (4), OO\*  $\rightarrow$  \* + O<sub>2</sub> (5), where \* stands out the catalytic site. Note that if oxygen cannot be chemisorbed on the site, the fourth step will be denoted as OOH\* + OH $^ \rightarrow$  \* + O<sub>2</sub> + H<sub>2</sub>O + e $^-$ , and the fifth step will not exist. The

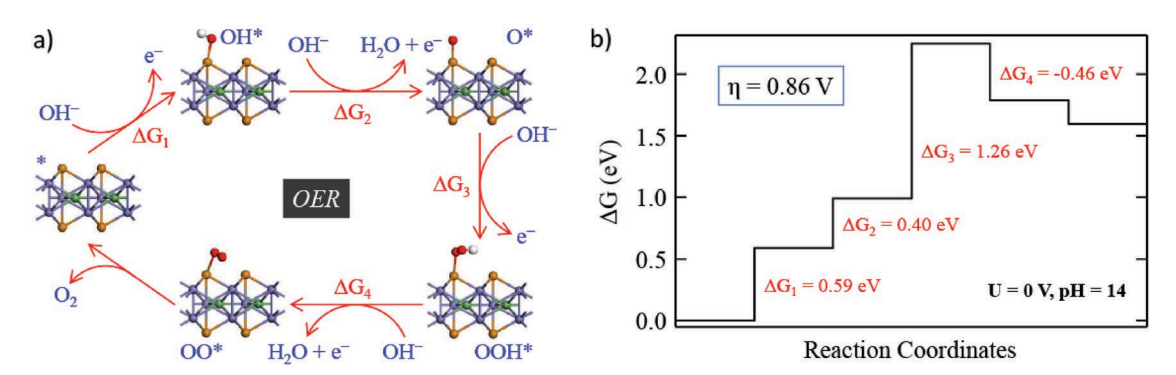


Figure 2. a) Classical pathway of OER on the basal plane of Fe<sub>3</sub>GeTe<sub>2</sub> under alkaline conditions and the configurations of the involved reaction intermediates. b) Free energy diagram at U = 0 V and pH = 14 along the pathway in a), where U and  $\eta$  represent the electrode potential and overpotential, respectively.

configurations of the involved OER intermediates are presented in **Figure 2**a. The adsorption bond lengths of intermediates OH\*, O\*, OOH\*, and OO\* are 2.045, 1.835, 2.153, and 2.253 Å, respectively (Table S3, Supporting Information).

Along the classical pathway, the overpotential of OER on  $\text{Fe}_3\text{GeTe}_2$  is 0.86 V.  $\Delta G_1$ ,  $\Delta G_2$ ,  $\Delta G_3$ , and  $\Delta G_4$  were calculated to be 0.59, 0.40, 1.26, and -0.46 eV, respectively (Figure 2b). Obviously, the third step, namely  $\text{O*} + \text{OH}^- \to \text{OOH*} + \text{e}^-$ , is the rate-limiting process, leading to an overpotential of 0.86 V (Figure 2b). In other words, the step involving the O–O combination determines the whole OER along the classical pathway. Such a large overpotential means that  $\text{Fe}_3\text{GeTe}_2$  is not an excellent OER electrocatalyst providing that the reaction proceeds along the classical pathway.

# 2.3. OER Activity of Fe<sub>3</sub>GeTe<sub>2</sub> along Surface Hydroxyl-Boosted Pathways

Though the classical pathway can well describe OER on a single catalytic site, but it may be difficult to depict the cases where OER occurs on two sites, such as the most commonly used noble metal oxide  ${\rm IrO_2}^{[75]}$  and  ${\rm RuO_2}^{[76]}$  the perovskite-type material  ${\rm CaMnO_3}^{[77]}$  and the Fe-doped NiOOH,  $^{[78]}$  one of the most efficient noble metal-free electrocatalyst under alkaline conditions.  $^{[78]}$  These cases involve the splitting of either  ${\rm H_2O}$  or hydroxyl ion on two neighboring sites, which is beyond the classical OER pathway.

Our above computations have shown that along the classical pathway, the combination of O\* and the hydroxyl ion into OOH\* is the rate-determining step, resulting in a large overpotential. Providing that the hydroxyl ion is split by two sites, i.e., the oxygen atom of the hydroxyl ion combines with O\* to achieve the O-O bonding while its hydrogen atom is captured by the neighboring site, will the overpotential be significantly reduced? Among the three possible sites to capture the hydrogen atoms (\*, O\*, and OH\*), energetically OH\* is the most favorable to combine with the hydrogen atom. Thus, such an OER pathway is named as surface hydroxyl-boosted pathway (**Figure 3**a,b). In the surface hydroxyl-boosted pathway, there are two possible ways to form the intermediate O\*+OH\*. In the first case (OH-boosted I, Figure 3a,c), O\*+OH\* is formed by  $2OH* + OH^- \rightarrow O*+OH* + H_2O + e^-$ , while in the second case

(OH-boosted II, Figure 3b,d), O\*+OH\* is generated by O\* + OH^  $\rightarrow$  O\*+OH\* + e^.

Following the OH-boosted I pathway, the OER overpotential on Fe<sub>3</sub>GeTe<sub>2</sub> can be reduced to 0.30 V. The adsorbed OH species on the Fe<sub>3</sub>GeTe<sub>2</sub> surface can stabilize the adsorption of the neighboring species. As shown in Figure 3a,c,  $\Delta G$  for OH\* +  $OH^- \rightarrow 2OH^* + e^-$  is only 0.22 eV, lower than that from \* to OH\* (see Figure 2). The adsorption bond lengths of surface hydroxyls of intermediate 20H\* are 2.171 and 1.964 Å, respectively (Table S3, Supporting Information). The next step is  $2OH^* + OH^- \rightarrow O^* + OH^* + H_2O + e^-$  (Figure 3a), and the calculated  $\Delta G$  is 0.28 eV (Figure 3c), which is also lower compared with  $\Delta G$  from OH\* to O\* (Figure 2). The lengths of two Te-O bonds of intermediate O\*+OH\* are 1.884 and 1.926 Å, respectively (Table S3, Supporting Information). From the configurations of the intermediates 20H\* and O\*+OH\* (Figure 3a), the lowered  $\Delta G$  should be due to the hydrogen bonding. If along the classical pathway, the following step will involve the O-O combination of the intermediate O\* and the hydroxyl ion accompanied by the electron transfer, namely  $O^*+OH^* + OH^- \rightarrow$ OOH\*+OH\* + e-. However, unlike the intermediate OOH\*, OOH\*+OH\* cannot survive and it will directly transform into OO\* and H<sub>2</sub>O by the structural optimization (Figure S5, Supporting Information). This process is extremely similar with OER proceeding on RuO2(110), where the intermediate OOH\*+O\* is also unstable and will barrierlessly transform into OO\*+OH\*. [76] As a result, similar to OER on RuO2(110), the following process should be denoted as  $O*+OH*+OH^- \rightarrow$  $OO^* + H_2O + e^-$  (Figure 3a) whose  $\Delta G$  was calculated to be 0.70 eV (Figure 3c). In other words, the O-O combination is accompanied by the electron transfer and the self-reduction of the adsorbed OH species into water. Obviously, the ratelimiting process along the OH-boosted I pathway (Figure 3a) is the step from O\*+OH\* to OO\* (Figure 3c) with  $\Delta G$  of 0.7 eV, and thus the overpotential is 0.30 V. Compared with the large overpotential determined from O\* to OOH\* (Figure 2), the selfreduction of the surface hydroxyl into water plays a crucial role in lowering the overpotential.

Following the OH-boosted II pathway, the overpotential for OER on Fe<sub>3</sub>GeTe<sub>2</sub> is also 0.30 V since the same rate determining step (O\*+OH\* + OH $^ \rightarrow$  OO\* + H<sub>2</sub>O + e $^-$ ) is involved. Like the classical pathway (Figure 2a), the first two steps of the OH-boosted II pathway are \* + OH $^ \rightarrow$  OH\* + e $^-$  and

www.advancedsciencenews.com www.afm-journal.de

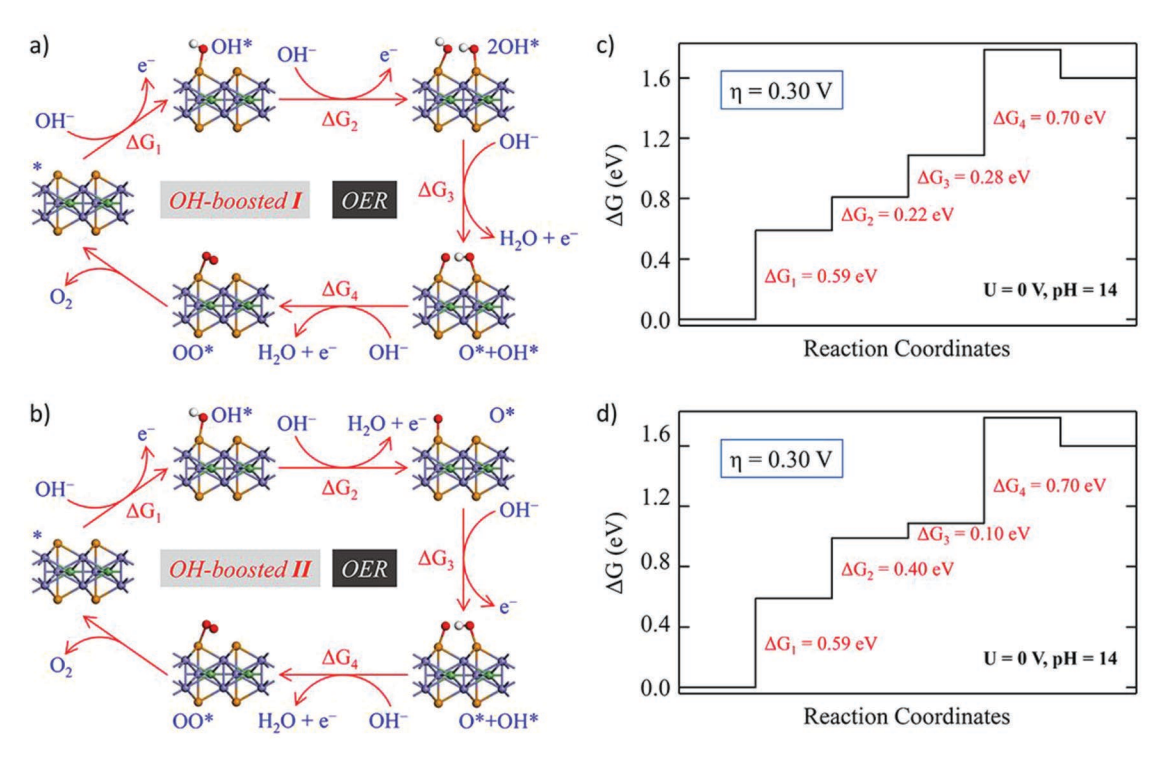


Figure 3. a,b) Surface-hydroxyl-boosted pathways of OER on the basal plane of Fe<sub>3</sub>GeTe<sub>2</sub> under alkaline conditions, together with the configurations of the involved reaction intermediates. c,d) Free energy diagrams at the conditions (U = 0 V and pH = 14) along the pathways in (a) and (b), respectively. The electrode potential and overpotential are denoted as U and  $\eta$ , respectively.

 $OH^* + OH^- \rightarrow O^* + H_2O + e^-$  (Figure 3b). Their  $\Delta G$  are 0.59 and 0.40 eV, respectively, as shown in Figure 3d. The following step is the formation of the intermediate O\*+OH\*, i.e., O\* +  $OH^- \rightarrow O^* + OH^* + e^-$  whose  $\Delta G$  is 0.10 eV (Figure 3b,d). The fourth step involves the O-O combination accompanied by the electron transfer and the self-reduction of surface hydroxyl into water (Figure 3b). The more details on the step have been discussed above, and its  $\Delta G$  was calculated to be 0.70 eV. Thus, the fourth step is still the rate-determining process (Figure 3d), resulting in the same overpotential as OER proceeding along the OH-boosted I pathway (Figure 3b).

Our conclusion that the self-reduction of surface hydroxyl into water can significantly boost the OER activity is obtained based on the ferromagnetic ground state. Note that the Curie temperature of Fe<sub>3</sub>GeTe<sub>2</sub> is 130 K,<sup>[59]</sup> below the room temperature at which the electrocatalysts are typically operated. As a result, Fe<sub>3</sub>GeTe<sub>2</sub> may not be in the ferromagnetic ground state when used as an electrocatalyst, and it may be in the nonferromagnetic state. However, according to our computations, the Curie temperature of Fe<sub>3</sub>GeTe<sub>2</sub> below room temperature has a very slight effect on the catalytic activity and does not affect our conclusion. More detailed discussion can be found in the Supporting Information.

Will the spin orientation of Fe<sub>3</sub>GeTe<sub>2</sub> affect the OER activity and metallicity? Note that Fe<sub>3</sub>GeTe<sub>2</sub> is inevitably exposed to the external electrical stimulation when applied as the OER electrocatalyst. Previous studies have shown that the external electrical stimulation can change the spin orientation of 2D magnets, [79,80] and the spin re-orientation was found to be able to modify the electronic properties.<sup>[81,82]</sup> Thus, it is necessary to

explore the effect of the spin reorientation of Fe<sub>3</sub>GeTe<sub>2</sub> on the OER activity and metallicity. Towards this end, we included the spin-orbit coupling (SOC) in our DFT calculations. Following the OH-boosted I pathway,  $\Delta G_1$ ,  $\Delta G_2$ , and  $\Delta G_3$  remain unchanged, and only  $\Delta G_4$  is increased by 0.01 eV when rotating the magnetic moment from out-of-plane (Figure 4a) to in-plane (Figure 4b). Such a tiny change demonstrates that the OER activity of Fe<sub>3</sub>GeTe<sub>2</sub> is insensitive to the spin direction. Similarly,  $\Delta G$  of OER along the OH-boosted II pathway are almost unchanged with the reorientation of the magnetic moment, as illustrated in Figure 4c,d. DOS analysis (Figure S6, Supporting Information) shows that the rotation of the spin direction does not break the metallic character of Fe<sub>3</sub>GeTe<sub>2</sub>. DOS of Fe<sub>3</sub>GeTe<sub>2</sub> with out-of-plane and in-plane spin orientations are of high similarity, which explains the tiny change of  $\Delta G$  with the spin reorientation well.

Multilayer Fe<sub>3</sub>GeTe<sub>2</sub> also owns high performance to catalyze OER following the same catalytic mechanism as the Fe<sub>3</sub>GeTe<sub>2</sub> monolayer. In general, it is difficult to obtain monolayer materials in the practical application, in particular for electrocatalysts. Therefore, we explored the catalytic performance and mechanism of the multilayer. Bilayer and trilayer Fe<sub>3</sub>GeTe<sub>2</sub> have high electrocatalytic performance towards OER with the overpotential of 0.33 V (Figures S7 and S8, Supporting Information). Like the monolayer (Figures 2 and 3), the self-reduction of surface hydroxyl into water can significantly reduce the overpotential for OER, thus greatly boosting the OER activity. Bilayer and trilayer Fe<sub>3</sub>GeTe<sub>2</sub> own the almost same free energy diagrams, which shows that the catalytic activity of Fe<sub>3</sub>GeTe<sub>2</sub> has been converged against the layer number. As a result, the

www.afm-journal.de

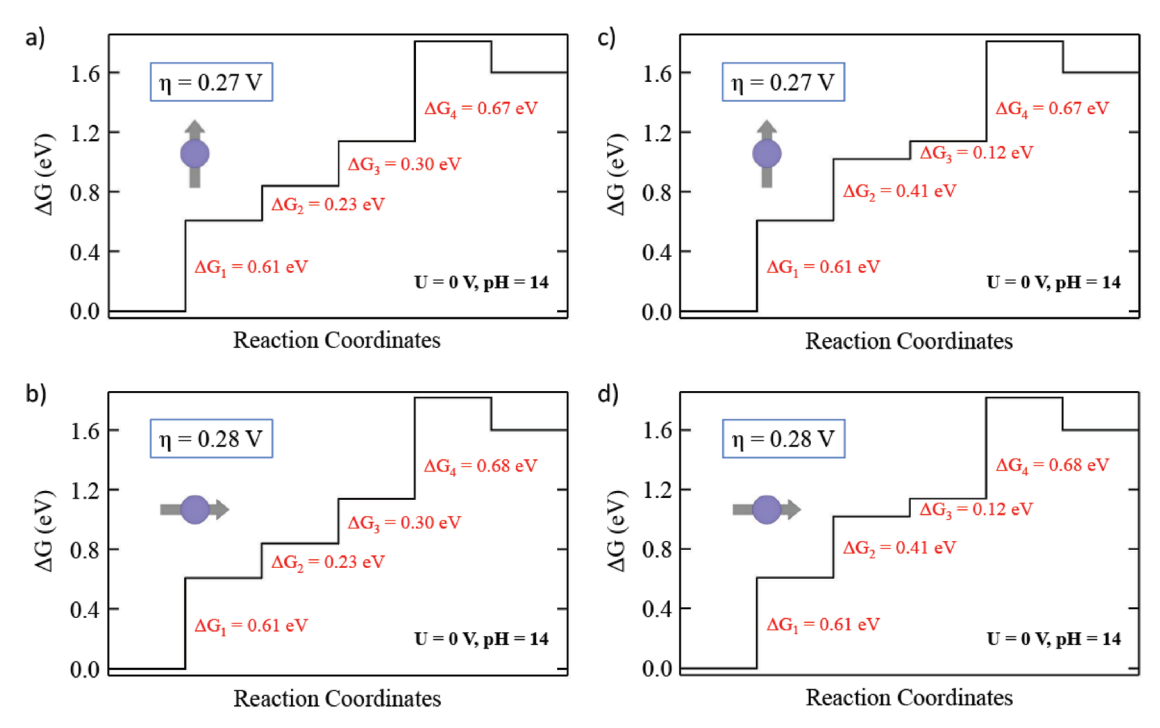


Figure 4. Free energy diagrams of OER on Fe<sub>3</sub>GeTe<sub>2</sub> with a,c) out-of-plane and b,d) in-plane spin orientations at U = 0 V and pH = 14 along OH-boosted a,b) I and c,d) II pathways, where U and η represent the electrode potential and overpotential, respectively.

catalytic activity of trilayer  $Fe_3GeTe_2$  can well represent that of the multilayer  $Fe_3GeTe_2$ . Note that the catalytic activity of bulk materials cannot be directly calculated in theory, and its activity is often approximated by that of multilayer. Thus, it is expected that bulk  $Fe_3GeTe_2$  also has high performance towards OER.

### 3. Conclusion

In summary, by means of DFT computations, we demonstrated that Fe<sub>3</sub>GeTe<sub>2</sub> nanosheet, one of emerging 2D ferromagnets, is an excellent OER electrocatalyst. Fe<sub>3</sub>GeTe<sub>2</sub> remains metallic from bulk to single layer, ensuring efficient electron transfer in Fe<sub>3</sub>GeTe<sub>2</sub> nanosheet during electrochemical reactions. The basal plane of ferromagnetic Fe<sub>3</sub>GeTe<sub>2</sub> is of high OER activity, on which OER can be driven with an overpotential of 0.30 V. Due to high specific surface area, electrocatalysts based on 2D vdW materials can offer abundant exposed catalytic sites. Together, these findings strongly suggest that Fe<sub>3</sub>GeTe<sub>2</sub> nanosheet could greatly advance the energy technologies related to electrochemical OER. Notably, for the first time, we revealed the self-reduction of surface hydroxyl can significantly boost the OER activity: surface hydroxyl can stabilize the adsorption of the neighboring species via hydrogen bonding, and the overpotential can be significantly lowered with surface hydroxyl self-reducing into water. Such insights not only promote the understanding of OER, but also open a new route for the design of OER electrocatalysts. This work is the first attempt to utilize the emerging 2D ferromagnets in the energy-related field, and we hope that it will stimulate more experimental and theoretical studies toward exploring the potential applications of emerging 2D ferromagnets in the growing field of energy storage and conversion.

# 4. Experimental Section

All spin-polarized DFT calculations were performed by using the Vienna ab initio simulation package<sup>[83]</sup> within the projected augmented wave method. [84] Local density approximation (LDA)[85] was adopted as the exchange-correlation functionals since previous theoretical and experimental studies have demonstrated that the LDA functional alone is sufficient to accurately describe the Fe<sub>3</sub>GeTe<sub>2</sub> system among all the tested exchange-correlation functionals.<sup>[58,64,86]</sup> Besides, the results obtained were provided by using Perdew-Burke-Enzerhof (PBE) generalized gradient approximation [87] (Figures S9-S11, Supporting Information). The calculated overpotential by PBE (0.39 V) is slightly larger than that obtained by LDA (0.30 V), but the OER mechanism revealed in this work, i.e., the overpotential can be remarkably lowered via the self-reduction of surface hydroxyl into water, is intrinsic and independent of the form of the functional, either LDA or PBE. The cut-off energy, the thickness of the vacuum space, and the k-point meshes for optimizing unit cells of single-layer, bilayer, trilayer, and bulk Fe<sub>3</sub>GeTe<sub>2</sub> are in accordance with the previous study.<sup>[58]</sup> For geometry optimizations of OER intermediates, a 2 × 2 supercell was used, and the Brillouin zone was sampled by using a  $5 \times 5 \times 1$  gamma-centered k-point mesh. The atomic positions in all the structures were fully relaxed until the energy change between two steps was less than  $10^{-5}$  eV and the forces acting on each atom was less than 0.01 eV Å-1.

Gibbs reaction free energy ( $\Delta G$ ) of each step was calculated by using the method developed by Nørskov and co-workers.  $^{[1.88-90]}$  According to their method,  $\Delta G$  is defined as follows:  $\Delta G = \Delta E + \Delta E_{ZPE} - T\Delta S - eU$ , in which  $\Delta E$  is the reaction energy directly obtained by DFT calculations,  $\Delta E_{ZPE}$  is the change in the zero-point energy, T is the reaction temperature (set to 298.15 K),  $\Delta S$  is the entropy difference, and U denotes the electrode potential with respect to the standard hydrogen electrode (SHE). Zero-point energies of the OER intermediates were derived from the vibration frequencies, and the entropy difference among the OER intermediates was neglected.  $^{[1.90]}$  The difference between the Gibbs free energies of OH $^-$  and  $e^-$  was calculated as  $G(OH-)-G(e-)=1/2G(H_2O)+1/4G(O_2)-0.40$  eV. 0.40 V represents the equilibrium reduction potential versus SHE for  $O_2$  to OH $^-$ , i.e.,  $O_2+2H_2O+4e^- \rightarrow 4OH^-$ ,

www.advancedsciencenews.com

www.afm-journal.de

at the conditions (T=298.15~K, P=1~bar, and pH=14). [91] Note that the high-spin ground state of  $O_2$  is notoriously poorly described in DFT calculations, so the Gibbs free energy of  $O_2$  was derived as  $G(O_2)=2G(H_2O)-2G(H_2)+4.92~\text{eV}.$ [1.88,90] Zero-point energies and entropies of  $H_2O$  and  $H_2$  were obtained from the previous study. [88] The OER activity is evaluated by the overpotential ( $\eta$ ):  $\eta=\Delta G_{\text{max}}/e-0.40~\text{V}$ .  $\Delta G_{\text{max}}$  is the maximum among  $\Delta G$  of all the reaction steps involving the electron transfer. The smaller the overpotential is, the higher the OER activity is.

## **Supporting Information**

Supporting Information is available from the Wiley Online Library or from the author.

# Acknowledgements

This work was financially supported by NASA (Grant No. 80NSSC17M0047) and NSF-CREST Center for Innovation, Research and Education in Environmental Nanotechnology (CIRE2N, Grant No. HRD-1736093). This research used resources of the High Performance of Computational facility (HPCf), University of Puerto Rico, which is partially supported by an Institutional Development Award (IDeA) INBRE Grant No. P20GM103475 from the National Institute of General Medical Sciences (NIGMS), a component of the National Institutes of Health (NIH), and the Bioinformatics Research Core of the INBRE. Its contents are solely the responsibility of the authors and do not necessarily represent the official view of NIH. A portion of this research used computational resources at the Center for Nanophase Materials Sciences, which is a DOE Office of Science User Facility.

#### **Conflict of Interest**

The authors declare no conflict of interest.

#### Keywords

2D ferromagnets, Fe<sub>3</sub>GeTe<sub>2</sub>, oxygen evolution reaction

Received: June 14, 2019 Revised: July 25, 2019 Published online:

- [1] L. C. Seitz, C. F. Dickens, K. Nishio, Y. Hikita, J. Montoya, A. Doyle, C. Kirk, A. Vojvodic, H. Y. Hwang, J. K. Nørskov, T. F. Jaramillo, Science 2016, 353, 1011.
- [2] H. Fei, J. Dong, Y. Feng, C. S. Allen, C. Wan, B. Volosskiy, M. Li, Z. Zhao, Y. Wang, H. Sun, P. An, W. Chen, Z. Guo, C. Lee, D. Chen, I. Shakir, M. Liu, T. Hu, Y. Li, A. I. Kirkland, X. Duan, Y. Huang, Nat. Catal. 2018, 1, 63.
- [3] E. Fabbri, M. Nachtegaal, T. Binninger, X. Cheng, B.-J. Kim, J. Durst, F. Bozza, T. Graule, R. Schäublin, L. Wiles, M. Pertoso, N. Danilovic, K. E. Ayers, T. J. Schmidt, *Nat. Mater.* 2017, 16, 925.
- [4] J. W. D. Ng, M. García-Melchor, M. Bajdich, P. Chakthranont, C. Kirk, A. Vojvodic, T. F. Jaramillo, Nat. Energy 2016, 1, 16053.
- [5] X. Lu, C. Zhao, Nat. Commun. 2015, 6, 6616.
- [6] S. Zhao, Y. Wang, J. Dong, C.-T. He, H. Yin, P. An, K. Zhao, X. Zhang, C. Gao, L. Zhang, J. Lv, J. Wang, J. Zhang, A. M. Khattak, N. A. Khan, Z. Wei, J. Zhang, S. Liu, H. Zhao, Z. Tang, *Nat. Energy* 2016, 1, 16184.

- [7] S. Geiger, O. Kasian, M. Ledendecker, E. Pizzutilo, A. M. Mingers, W. T. Fu, O. Diaz-Morales, Z. Li, T. Oellers, L. Fruchter, A. Ludwig, K. J. J. Mayrhofer, M. T. M. Koper, S. Cherevko, *Nat. Catal.* 2018, 1, 508
- [8] A. Grimaud, A. Demortiere, M. Saubanere, W. Dachraoui, M. Duchamp, M.-L. Doublet, J.-M. Tarascon, Nat. Energy 2017, 2, 16189
- [9] L. Yang, G. Yu, X. Ai, W. Yan, H. Duan, W. Chen, X. Li, T. Wang, C. Zhang, X. Huang, J.-S. Chen, X. Zou, *Nat. Commun.* 2018, 9, 5226
- [10] S. Zhao, M. Li, M. Han, D. Xu, J. Yang, Y. Lin, N.-E. Shi, Y. Lu, R. Yang, B. Liu, Z. Dai, J. Bao, Adv. Funct. Mater. 2018, 28, 1706018.
- [11] C. Copéret, M. Chabanas, R. Petroff Saint-Arroman, J.-M. Basset, Angew. Chem., Int. Ed. 2003, 42, 156.
- [12] D. Astruc, F. Lu, J. R. Aranzaes, Angew. Chem., Int. Ed. 2005, 44, 7852
- [13] K. S. Novoselov, A. K. Geim, S. V. Morozov, D. Jiang, Y. Zhang, S. V. Dubonos, I. V. Grigorieva, A. A. Firsov, Science 2004, 306, 666.
- [14] H. Li, C. Tsai, A. L. Koh, L. Cai, A. W. Contryman, A. H. Fragapane, J. Zhao, H. S. Han, H. C. Manoharan, F. Abild-Pedersen, J. K. Nørskov, X. Zheng, *Nat. Mater.* 2016, 15, 48.
- [15] D. Voiry, R. Fullon, J. Yang, E. S. C. de Carvalho Castro, R. Kappera,
  I. Bozkurt, D. Kaplan, M. J. Lagos, P. E. Batson, G. Gupta,
  A. D. Mohite, L. Dong, D. Er, V. B. Shenoy, T. Asefa, M. Chhowalla,
  Nat. Mater. 2016, 15, 1003.
- [16] Y. Liu, J. Wu, K. P. Hackenberg, J. Zhang, Y. M. Wang, Y. Yang, K. Keyshar, J. Gu, T. Ogitsu, R. Vajtai, J. Lou, P. M. Ajayan, B. C. Wood, B. I. Yakobson, *Nat. Energy* 2017, 2, 17127.
- [17] Y. Wang, Y. Li, T. Heine, J. Am. Chem. Soc. 2018, 140, 12732.
- [18] C. Zhu, D. Gao, J. Ding, D. Chao, J. Wang, *Chem. Soc. Rev.* **2018**, 47, 4332
- [19] J. Deng, H. Li, J. Xiao, Y. Tu, D. Deng, H. Yang, H. Tian, J. Li, P. Ren, X. Bao, Energy Environ. Sci. 2015, 8, 1594.
- [20] Y. Li, H. Su, S. H. Chan, Q. Sun, ACS Catal. 2015, 5, 6658.
- [21] Z. Zhao, Z. Xia, ACS Catal. 2016, 6, 1553.
- [22] G. Gao, Y. Jiao, E. R. Waclawik, A. Du, J. Am. Chem. Soc. 2016, 138, 6292.
- [23] X.-F. Li, Q.-K. Li, J. Cheng, L. Liu, Q. Yan, Y. Wu, X.-H. Zhang, Z.-Y. Wang, Q. Qiu, Y. Luo, J. Am. Chem. Soc. 2016, 138, 8706.
- [24] X. Tan, H. A. Tahini, S. C. Smith, ACS Catal. 2016, 6, 7071.
- [25] Y. Jiao, Y. Zheng, P. Chen, M. Jaroniec, S.-Z. Qiao, J. Am. Chem. Soc. 2017, 139, 18093.
- [26] Y. Shi, Y. Zhou, D.-R. Yang, W.-X. Xu, C. Wang, F.-B. Wang, J.-J. Xu, X.-H. Xia, H.-Y. Chen, J. Am. Chem. Soc. 2017, 139, 15479.
- [27] C. Ling, X. Niu, Q. Li, A. Du, J. Wang, J. Am. Chem. Soc. 2018, 140, 14161.
- [28] H. Xu, D. Cheng, D. Cao, X. C. Zeng, Nat. Catal. 2018, 1, 339.
- [29] Q.-K. Li, X.-F. Li, G. Zhang, J. Jiang, J. Am. Chem. Soc. 2018, 140, 15149.
- [30] Y. Zhao, J. Wan, H. Yao, L. Zhang, K. Lin, L. Wang, N. Yang, D. Liu, L. Song, J. Zhu, L. Gu, L. Liu, H. Zhao, Y. Li, D. Wang, *Nat. Chem.* 2018, 10, 924.
- [31] Z. Luo, Y. Ouyang, H. Zhang, M. Xiao, J. Ge, Z. Jiang, J. Wang, D. Tang, X. Cao, C. Liu, W. Xing, Nat. Commun. 2018, 9, 2120.
- [32] C. Liu, Q. Li, C. Wu, J. Zhang, Y. Jin, D. R. MacFarlane, C. Sun, J. Am. Chem. Soc. 2019, 141, 2884.
- [33] W. Zhao, L. Zhang, Q. Luo, Z. Hu, W. Zhang, S. Smith, J. Yang, ACS Catal. 2019, 9, 3419.
- [34] Y. Qin, H.-H. Wu, L. A. Zhang, X. Zhou, Y. Bu, W. Zhang, F. Chu, Y. Li, Y. Kong, Q. Zhang, D. Ding, Y. Tao, Y. Li, M. Liu, X. C. Zeng, ACS Catal. 2019, 9, 610.
- [35] Z. Zhu, H. Yin, C.-T. He, M. Al-Mamun, P. Liu, L. Jiang, Y. Zhao, Y. Wang, H.-G. Yang, Z. Tang, D. Wang, X.-M. Chen, H. Zhao, Adv. Mater. 2018, 30, 1801171.

www.advancedsciencenews.com www.afm-journal.de

- [36] C. Li, Y. Liu, Z. Zhuo, H. Ju, D. Li, Y. Guo, X. Wu, H. Li, T. Zhai, Adv. Energy Mater. 2018, 8, 1801775.
- [37] M.-R. Gao, J.-X. Liang, Y.-R. Zheng, Y.-F. Xu, J. Jiang, Q. Gao, J. Li, S.-H. Yu, Nat. Commun. 2015, 6, 5982.
- [38] Y. Yin, J. Han, Y. Zhang, X. Zhang, P. Xu, Q. Yuan, L. Samad, X. Wang, Y. Wang, Z. Zhang, P. Zhang, X. Cao, B. Song, S. Jin, J. Am. Chem. Soc. 2016, 138, 7965.
- [39] Y. Ouyang, C. Ling, Q. Chen, Z. Wang, L. Shi, J. Wang, Chem. Mater. 2016, 28, 4390.
- [40] Y. Bao, M. Yang, S. J. R. Tan, Y. P. Liu, H. Xu, W. Liu, C. T. Nai, Y. P. Feng, J. Lu, K. P. Loh, J. Am. Chem. Soc. 2016, 138, 14121.
- [41] G. Li, D. Zhang, Q. Qiao, Y. Yu, D. Peterson, A. Zafar, R. Kumar, S. Curtarolo, F. Hunte, S. Shannon, Y. Zhu, W. Yang, L. Cao, J. Am. Chem. Soc. 2016, 138, 16632.
- [42] G. Ye, Y. Gong, J. Lin, B. Li, Y. He, S. T. Pantelides, W. Zhou, R. Vajtai, P. M. Ajayan, *Nano Lett.* 2016, 16, 1097.
- [43] D. Li, Y. Jia, G. Chang, J. Chen, H. Liu, J. Wang, Y. Hu, Y. Xia, D. Yang, X. Yao, Chem 2018, 4, 2345.
- [44] J. Zhang, M. Ren, L. Wang, Y. Li, B. I. Yakobson, J. M. Tour, Adv. Mater. 2018, 30, 1707319.
- [45] C. Gong, L. Li, Z. Li, H. Ji, A. Stern, Y. Xia, T. Cao, W. Bao, C. Wang, Y. Wang, Z. Q. Qiu, R. J. Cava, S. G. Louie, J. Xia, X. Zhang, *Nature* 2017, 546, 265.
- [46] B. Huang, G. Clark, E. Navarro-Moratalla, D. R. Klein, R. Cheng, K. L. Seyler, D. Zhong, E. Schmidgall, M. A. McGuire, D. H. Cobden, W. Yao, D. Xiao, P. Jarillo-Herrero, X. Xu, *Nature* 2017, 546, 270.
- [47] K. S. Burch, D. Mandrus, J.-G. Park, Nature 2018, 563, 47.
- [48] C. Gong, X. Zhang, Science 2019, 363, eaav4450.
- [49] D. L. Cortie, G. L. Causer, K. C. Rule, H. Fritzsche, W. Kreuzpaintner, F. Klose, Adv. Funct. Mater., https://doi.org/10.1002/ adfm.201901414.
- [50] H. Li, S. Ruan, Y.-J. Zeng, Adv. Mater. 2019, 31, 1900065.
- [51] J. Zhu, M. Chen, H. Qu, Z. Luo, S. Wu, H. A. Colorado, S. Wei, Z. Guo, Energy Environ. Sci. 2013, 6, 194.
- [52] J. Zhu, M. Chen, H. Wei, N. Yerra, N. Haldolaarachchige, Z. Luo, D. P. Young, T. C. Ho, S. Wei, Z. Guo, Nano Energy 2014, 6, 180.
- [53] L. Wang, H. Yang, J. Yang, Y. Yang, R. Wang, S. Li, H. Wang, S. Ji, Ionics 2016, 22, 2195.
- [54] Z. Zeng, T. Zhang, Y. Liu, W. Zhang, Z. Yin, Z. Ji, J. Wei, ChemSusChem 2018, 11, 580.
- [55] N. Miao, B. Xu, L. Zhu, J. Zhou, Z. Sun, J. Am. Chem. Soc. 2018, 140, 2417.
- [56] C. Huang, J. Feng, F. Wu, D. Ahmed, B. Huang, H. Xiang, K. Deng, E. Kan, J. Am. Chem. Soc. 2018, 140, 11519.
- [57] X. Li, J. Yang, J. Am. Chem. Soc. 2019, 141, 109.
- [58] Y. Deng, Y. Yu, Y. Song, J. Zhang, N. Z. Wang, Z. Sun, Y. Yi, Y. Z. Wu, S. Wu, J. Zhu, J. Wang, X. H. Chen, Y. Zhang, *Nature* 2018, 563, 94.
- [59] Z. Fei, B. Huang, P. Malinowski, W. Wang, T. Song, J. Sanchez, W. Yao, D. Xiao, X. Zhu, A. F. May, W. Wu, D. H. Cobden, J.-H. Chu, X. Xu, Nat. Mater. 2018, 17, 778.
- [60] Q. Li, M. Yang, C. Gong, R. V. Chopdekar, A. T. N'Diaye, J. Turner, G. Chen, A. Scholl, P. Shafer, E. Arenholz, A. K. Schmid, S. Wang, K. Liu, N. Gao, A. S. Admasu, S.-W. Cheong, C. Hwang, J. Li, F. Wang, X. Zhang, Z. Qiu, Nano Lett. 2018, 18, 5974.
- [61] H.-J. Deiseroth, K. Aleksandrov, C. Reiner, L. Kienle, R. K. Kremer, Eur. J. Inorg. Chem. 2006, 2006, 1561.

- [62] K. Aleksandrov, Ph.D. Thesis, Universität Siegen 2005.
- [63] B. Chen, J. Yang, H. Wang, M. Imai, H. Ohta, C. Michioka, K. Yoshimura, M. Fang, J. Phys. Soc. Jpn. 2013, 82, 124711.
- [64] H. L. Zhuang, P. R. C. Kent, R. G. Hennig, Phys. Rev. B 2016, 93, 134407.
- [65] J. Qiao, X. Kong, Z.-X. Hu, F. Yang, W. Ji, Nat. Commun. 2014, 5, 4475.
- [66] Y. Cai, G. Zhang, Y.-W. Zhang, Sci. Rep. 2015, 4, 6677.
- [67] L. Kou, C. Chen, S. C. Smith, J. Phys. Chem. Lett. 2015, 6, 2794.
- [68] S. Zhang, Z. Yan, Y. Li, Z. Chen, H. Zeng, Angew. Chem., Int. Ed. 2015, 54, 3112.
- [69] M. Hafeez, L. Gan, H. Li, Y. Ma, T. Zhai, Adv. Funct. Mater. 2016, 26, 4551.
- [70] X. Zhang, X. Zhao, D. Wu, Y. Jing, Z. Zhou, Adv. Sci. 2016, 3, 1600062.
- [71] Y. Jing, Y. Ma, Y. Li, T. Heine, Nano Lett. 2017, 17, 1833.
- [72] N. Miao, B. Xu, N. C. Bristowe, J. Zhou, Z. Sun, J. Am. Chem. Soc. 2017, 139, 11125.
- [73] X. Zhou, X. Hu, J. Yu, S. Liu, Z. Shu, Q. Zhang, H. Li, Y. Ma, H. Xu, T. Zhai, Adv. Funct. Mater. 2018, 28, 1706587.
- [74] N. T. Suen, S.-F. Hung, Q. Quan, N. Zhang, Y.-J. Xu, H. M. Chen, Chem. Soc. Rev. 2017, 46, 337.
- [75] Y. Ping, R. J. Nielsen, W. A. Goddard, J. Am. Chem. Soc. 2017, 139, 149.
- [76] R. R. Rao, M. J. Kolb, N. B. Halck, A. F. Pedersen, A. Mehta, H. You, K. A. Stoerzinger, Z. Feng, H. A. Hansen, H. Zhou, L. Giordano, J. Rossmeisl, T. Vegge, I. Chorkendorff, I. E. L. Stephens, Y. Shao-Horn, Energy Environ. Sci. 2017, 10, 2626.
- [77] T. Qiu, B. Tu, D. Saldana-Greco, A. M. Rappe, ACS Catal. 2018, 8, 2218.
- [78] H. Shin, H. Xiao, W. A. Goddard, J. Am. Chem. Soc. 2018, 140, 6745.
- [79] F. Zheng, J. Zhao, Z. Liu, M. Li, M. Zhou, S. B. Zhang, P. Zhang, Nanoscale 2018, 10, 14298.
- [80] J. He, G. Ding, C. Zhong, S. Li, D. Li, G. Zhang, Nanoscale 2019, 11, 356.
- [81] S. Zhang, R. Xu, W. Duan, X. Zou, Adv. Funct. Mater. 2019, 29, 1808380.
- [82] P. Jiang, L. Li, Z. Liao, Y. X. Zhao, Z. Zhong, Nano Lett. 2018, 18, 3844.
- [83] G. Kresse, J. Furthmüller, Phys. Rev. B 1996, 54, 11169.
- [84] P. E. Blöchl, Phys. Rev. B 1994, 50, 17953.
- [85] J. P. Perdew, A. Zunger, Phys. Rev. B 1981, 23, 5048.
- [86] Y. Zhang, H. Lu, X. Zhu, S. Tan, W. Feng, Q. Liu, W. Zhang, Q. Chen, Y. Liu, X. Luo, D. Xie, L. Luo, Z. Zhang, X. Lai, Sci. Adv. 2018, 4, eaao6791.
- [87] J. P. Perdew, K. Burke, M. Ernzerhof, Phys. Rev. Lett. 1996, 77, 3865.
- [88] J. K. Nørskov, J. Rossmeisl, A. Logadottir, L. Lindqvist, J. R. Kitchin, T. Bligaard, H. Jónsson, J. Phys. Chem. B 2004, 108, 17886.
- [89] B. Hinnemann, P. G. Moses, J. Bonde, K. P. Jørgensen, J. H. Nielsen, S. Horch, I. Chorkendorff, J. K. Nørskov, J. Am. Chem. Soc. 2005, 127, 5308.
- [90] M. Bajdich, M. García-Mota, A. Vojvodic, J. K. Nørskov, A. T. Bell, J. Am. Chem. Soc. 2013, 135, 13521.
- [91] X. Ge, A. Sumboja, D. Wuu, T. An, B. Li, F. W. Thomas Goh, T. S. Andy Hor, Y. Zong, Z. Liu, ACS Catal. 2015, 5, 4643.